2. D. Byers, R. Davis, J. Kiger, *Nature* **289**, 79 (1981); M. Livingstone, P. Sziber, W. Quinn, *Cell* **37**, 205 (1984); P. Drain, E. Folkers, W. Quinn, *Neuron* **6**, 71 (1991); Z. L. Wu *et al.*, *Proc. Natl. Acad. Sci. U.S.A.* **92**, 220 (1995); W. Li, T. Tully, D. Kalderon, *Learn. Mem.* **2**, 320 (1996).
3. E. Skoulakis, D. Kalderon, R. Davis, *Neuron* **11**, 197 (1993).
4. A. Nighorn, M. Healy, R. Davis, *ibid.* **6**, 455 (1991); P. Han, L. Levin, R. Reed, R. Davis, *ibid.* **9**, 619 (1992).
5. M. Heisenberg, A. Borst, S. Wagner, D. Byers, *J. Neurogenet.* **2**, 1 (1985); J. S. de Belle and M. Heisenberg, *Proc. Natl. Acad. Sci. U.S.A.* **93**, 9875 (1996).
6. J. S. de Belle and M. Heisenberg, *Science* **263**, 692 (1994).
7. A. Brand and N. Perrimon, *Development* **118**, 401 (1993).
8. F. Quan, W. Wolfgang, M. Forte, *Proc. Natl. Acad. Sci. U.S.A.* **86**, 4321 (1989); W. Wolfgang *et al.*, *J. Neurosci.* **10**, 1014 (1990).
9. F. Quan, L. Thomas, M. Forte, *Proc. Natl. Acad. Sci. U.S.A.* **88**, 1898 (1991).
10. M. Simon, M. Strathmann, N. Gautam, *Science* **252**, 802 (1991); H. Bourne, D. Sanders, F. McCormick, *Nature* **349**, 117 (1991); W. Tang and A. Gilman, *Cell* **70**, 869 (1992); A. Spiegel *et al.*, in *G Proteins* (Molecular Biology Intelligence Unit, R. G. Landes Co., Austin, TX, 1994), pp. 19–20; E. Neer, *Cell* **60**, 249 (1995).
11. Complementary DNAs encoding the short forms of $G\alpha_s$WT and $G\alpha_s$* (*9*) were subcloned into pUAST (*7*) and used to transform flies [A. Spradling, in *Drosophila: A Practical Approach*, D. Roberts, Ed. (IRL Press, Oxford, 1986), pp. 75–197]. The UAS-$G\alpha_s$ lines were verified by Msc I digestion of polymerase chain reaction–amplified $G\alpha_s$ transgenes to detect the presence of a site found in $G\alpha_s$WT but lacking as a result of the Q215L mutation.
12. 238Y and 201Y are described in (*17*) and C232 in (*18*). C747 shows identical expression to that of C772 (*17*) (*24*). C309 is described by J. D. Armstrong [thesis, University of Glasgow, Scotland (1995)]. The O'Kane laboratory screened 500 P-GAL4 lines to identify OK66, OK86, OK62, OK107, OK348, and OK415.
13. T. Tully and W. Quinn, *J. Comp. Physiol.* **157**, 263 (1985); T. Tully, T. Preat, S. Boynton, M. Del Vecchio, *Cell* **79**, 35 (1994).
14. In total, we analyzed behaviorally 16 P-GAL4 insertions that expressed to some degree in MBs. Flies with four insertions (OK66, OK86, KL65, and KL107) showed reduced learning in the absence of expression of constitutively activated $G\alpha_s$*, most likely because of genetic background differences. These were not tested further. Flies with eight insertions showed defects in olfactory acuity (30Y, C35, OK62, OK107, C302, OK415, and C532) or shock reactivity (C772), as transheterozygotes with UAS-$G\alpha_s$*. These were eliminated from further behavioral testing. Flies with the remaining four P-GAL4 insertions (201Y, 238Y, C309, and C747) showed disrupted learning but normal olfactory acuity and shock reactivity, as transheterozygotes with at least one UAS-$G\alpha_s$* insertion. We characterized a total of two P-GAL4 insertions (C232 and OK348) that expressed to some degree in the CC.
15. We suggest that olfactory learning results from G_s-dependent convergence of the conditional stimulus (CS) and unconditional stimulus (US) in the MBs. This belief is reinforced by the observation that expression of $G\alpha_s$* in the CC does not affect learning. Formally, however, we cannot exclude the possibility that other sites of convergence of the CS and US contribute to the conditioned behavior, as in honeybees [M. Hammer and R. Menzel, *J. Neurosci.* **15**, 1617 (1995)].
16. Direct immunolocalization of transgenic $G\alpha_s$ forms proved impossible, as endogenous $G\alpha_s$ is expressed throughout the central nervous system (*8*). We have not observed any significant differences in qualitative expression between UAS-regulated insertions [see also (*18*) and D. Lin and C. Goodman, *Neuron* **13**, 507 (1994)]. Thus, P-GAL4–driven reporter gene expression should reflect genuine expression patterns of $G\alpha_s$* under UAS regulation.
17. M. Y. Yang, J. D. Armstrong, I. Vilinsky, N. Strausfield, K. Kaiser, *Neuron* **15**, 45 (1995).
18. K. O'Dell, J. Armstrong, M. Y. Yang, K. Kaiser, *ibid.*, p. 55.
19. Pan-neural expression was driven by P-GAL4 1407 [generated by J. Urban and G. Technau; described in L. Luo, Y. Liao, L. Jan, Y. Jan, *Genes Dev.* **8**, 1787 (1994)].
20. The P-GAL4 C309 line was crossed to UAS-lacZ and UAS-lacZ;UAS-$G\alpha_s$* lines. Brains from the resultant progeny were dissected, and β-Gal activity was detected as described [S. T. Sweeney, K. Broadie, J. Keane, H. Niemann, C. J. O'Kane, *Neuron* **14**, 341 (1995)].
21. L. Levin *et al.*, *Cell* **68**, 479 (1992).
22. D. Cooper, N. Mons, J. Karpen, *Nature* **374**, 421 (1995).
23. D. Clapman, *Annu. Rev. Neurosci.* **17**, 441 (1994); W. Schreibmayer *et al.*, *Nature* **380**, 624 (1996).
24. K. Kaiser, unpublished data.
25. S. Boynton and T. Tully, *Genetics* **131**, 655 (1992).
26. R. Sokal and F. Rohlf, in *Biometry* (Freeman, New York, 1981), pp. 229–240.
27. E. Yeh, K. Gustafson, G. Boulianne, *Proc. Natl. Acad. Sci. U.S.A.* **92**, 7036 (1995).
28. L. Luo, T. Tully, K. White, *Neuron* **9**, 595 (1992).

29. We thank K. Moffat, J. Keane, K. Störtkuhl, R. Greenspan, M. Yang, G. Boulianne, and A. Brand for reagents. Supported by grants from the Wellcome Trust and the Science and Engineering Research Council (GR/F94989) (to C.J.O'K.), the Human Frontiers Science program (to C.J.O'K., K.K., and M.F.), and NIH grant HD 32245 (to T.T.).

3 June 1996; accepted 21 October 1996

A Mechanism of Drug Action Revealed by Structural Studies of Enoyl Reductase

Clair Baldock, John B. Rafferty, Svetlana E. Sedelnikova, Patrick J. Baker, Antoine R. Stuitje, Antoni R. Slabas, Timothy R. Hawkes, David W. Rice*

Enoyl reductase (ENR), an enzyme involved in fatty acid biosynthesis, is the target for antibacterial diazaborines and the front-line antituberculosis drug isoniazid. Analysis of the structures of complexes of *Escherichia coli* ENR with nicotinamide adenine dinucleotide and either thienodiazaborine or benzodiazaborine revealed the formation of a covalent bond between the 2′ hydroxyl of the nicotinamide ribose and a boron atom in the drugs to generate a tight, noncovalently bound bisubstrate analog. This analysis has implications for the structure-based design of inhibitors of ENR, and similarities to other oxidoreductases suggest that mimicking this molecular linkage may have generic applications in other areas of medicinal chemistry.

ENR catalyzes the final reaction of the fatty acid synthase cycle: the reduction of a carbon-carbon double bond in an enoyl moiety that is covalently linked to an acyl carrier protein. Recent studies have identified ENR as the target for a number of therapeutic agents against *Mycobacterium tuberculosis* (*1*) and *Escherichia coli* (*2*). *Mycobacterium tuberculosis* ENR is the target for a metabolite of isoniazid, a potent drug that is used in the front-line chemotherapeutic treatment of tuberculosis. However, strains of *M. tuberculosis* are emerging that are resistant to isoniazid (*3*), with consequent problems in treatment. *Escherichia coli* ENR is inhibited by a range of diazaborines, heterocyclic boron-containing compounds whose action is thought to lead to the inhibition of cell growth by preventing lipopolysaccharide synthesis (*4*). Biochemical studies on *E. coli* ENR have shown that nicotinamide adenine dinucleotide (NAD^+) is required for diazaborine binding; this finding has led to the suggestion that the drug binds to ENR in association with NAD^+ or that NAD^+ converts the drug to an active form (*5*). To obtain a molecular explanation for the inhibitory activities of this class of antibacterial agents, we determined and analyzed the structure of *E. coli* ENR in complexes with NAD^+ and either thienodiazaborine or benzodiazaborine as well as with NAD^+ alone.

The structure of the ENR-NAD^+ complex was solved to 2.1 Å (*6*); those of the ENR-NAD^+-thienodiazaborine and ENR-NAD^+-benzodiazaborine complexes were solved to 2.2 and 2.5 Å, respectively (*7*) (Table 1 and Fig. 1A). In the final map of the ENR-NAD^+ complex, the electron density is of high quality for most of the protein atoms. However, there is a break in the density for a stretch of 10 amino acid residues; these 10 residues form a loop between

C. Baldock, J. B. Rafferty, S. E. Sedelnikova, P. J. Baker, D. W. Rice, Krebs Institute for Biomolecular Research, Department of Molecular Biology and Biotechnology, University of Sheffield, Sheffield S10 2TN, UK.
A. R. Stuitje, Department of Genetics, Institute of Molecular Biological Studies (IMBW), Vrije Universiteit, Biocenter Amsterdam, De Boelelaan 1087, 1081 HV Amsterdam, Netherlands.
A. R. Slabas, Department of Biological Sciences, University of Durham, Durham DH1 3LE, UK.
T. R. Hawkes, Department of Exploratory Plant Sciences, Zeneca Agrochemicals, Jealott's Hill Research Station, Bracknell, Berkshire RG12 6EY, UK.

*To whom correspondence should be addressed. E-mail: D.Rice@sheffield.ac.uk

strand β6 and helix α6, that borders the nucleotide-binding site. In the structures of the ENR-NAD$^+$-diazaborine complexes, this loop is well defined and provides two residues whose side chains are in van der Waals contact with the non–boron-containing five- and six-membered rings of thienodiazaborine and benzodiazaborine, respectively.

The quality of the electron density map for both diazaborines enabled the unambiguous positioning of the bicyclic thienodiazaborine or benzodiazaborine rings, the sulfonyl groups, and the respective propyl or tosyl substituents (Fig. 1, B and C). Both diazaborine compounds bind in a closely related manner, adjacent to the nicotinamide ring of the cofactor, in a pocket formed by the side chains of Tyr^{146}, Tyr^{156}, Met^{159}, Ile^{200}, Phe^{203}, Leu^{100}, Lys^{163}, and the main-chain peptide between Gly^{93} and Ala^{95}. The bicyclic rings of the diazaborines form a face-to-face interaction with the nicotinamide ring, allowing the formation of extensive π-π stacking interactions with additional van der Waals interactions between the rings and the side chains of Tyr^{156}, Tyr^{146}, Phe^{203}, and Ile^{200}. The major difference between the binding of the two diazaborines is that their respective tosyl and propyl groups occupy subtly different positions. The tosyl moiety lies perpendicular to the bicyclic ring and interacts with the main chain peptide between Gly^{93} and Ala^{95} and the side chain of Leu^{100}, whereas the propyl moiety folds back onto the planar bicyclic ring system in a manner reminiscent of a scorpion's tail and forms interactions with the side chain of Met^{159} and Ile^{200} and the main chain peptide of both Gly^{93} and Phe^{94}. Additional interactions made by both drugs include hydrogen bonds between the boron hydroxyl and the phenolic hydroxyl of Tyr^{156} (Fig. 2) and between a nitrogen in the boron-containing ring and an ordered solvent molecule.

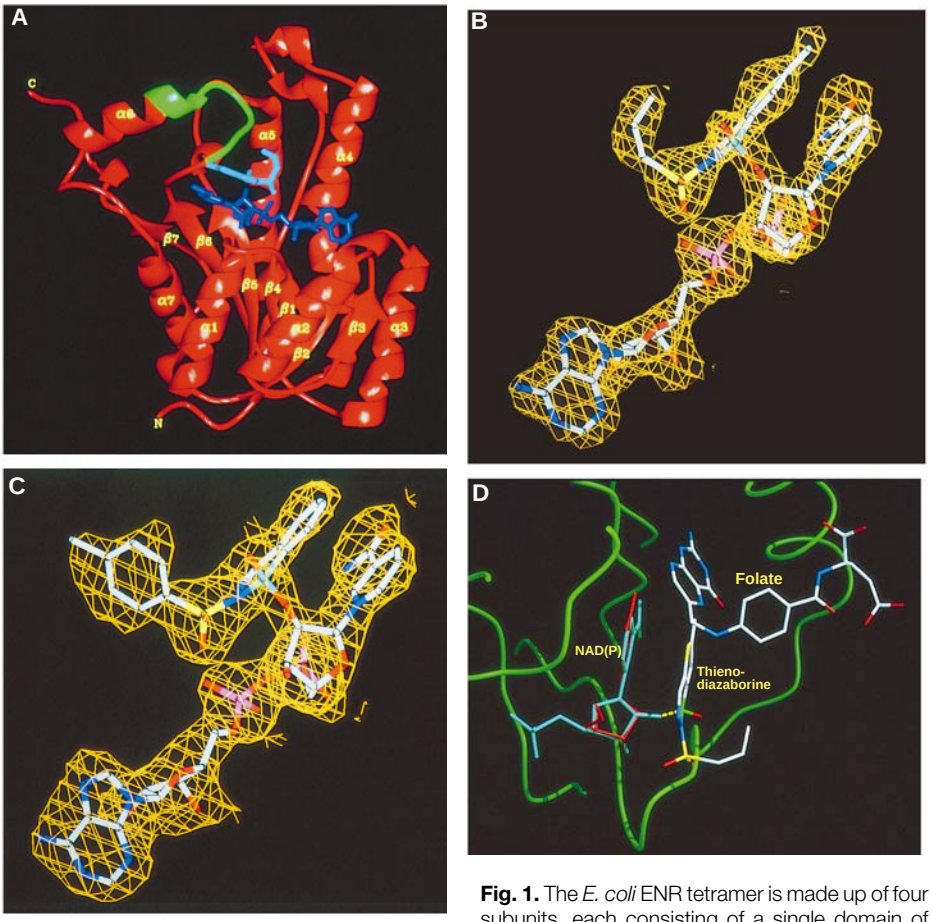

Fig. 1. The *E. coli* ENR tetramer is made up of four subunits, each consisting of a single domain of approximate dimensions 55 by 45 by 45 Å composed of a parallel β sheet of seven strands (β1 to β7), flanked on one side by helices α1, α2, and α7 and on the other by helices α3 to α5, with a further helix, α6, lying along the top of the β sheet. (**A**) Schematic diagram of a single subunit of the ENR-NAD$^+$-thienodiazaborine complex. The ribbon trace of *E. coli* ENR is shown in red; NAD$^+$ (blue) and diazaborine (cyan) are shown in an all-atom representation. The loop that orders on diazaborine binding is highlighted in green. [Produced using MIDAS (*25*).] (**B** and **C**) Initial Fourier maps of the NAD$^+$-thienodiazaborine complex at 2.2 Å resolution (B) and of the NAD$^+$-benzodiazaborine complex at 2.5 Å resolution (C) with the final refined structures superimposed. The density (contoured at 1.2σ and 0.9σ, respectively) was calculated with coefficients $2|F_{obs}| - |F_{calc}|$ and phases that were calculated from the refined structure from the molecular replacement solution that had been generated with the model of the *E. coli* ENR-NAD$^+$ complex, which contained no information about the inhibitor. [Produced using BOBSCRIPT (*26*), a modified version of MOLSCRIPT (*27*).] (**D**) The superposition (based on the nicotinamide and its associated ribose) of the nucleotide-inhibitor complex of ENR into the active site of the nucleotide-substrate complex of DHFR [PDB entry 7DFR (*13*)]. The Cα backbone trace for DHFR is shown in green, with bound NADP and folate colored turquoise and by atom, respectively; the superimposed NAD$^+$ and thienodiazaborine of ENR are shown in red and all atom colors, respectively (red, oxygen; white, carbon; blue, nitrogen; yellow, sulfur; green, boron). The covalent bond between the 2′ hydroxyl of the nicotinamide ribose and the boron of the diazaborine in ENR is represented by a dotted yellow line. [Produced using MIDAS (*25*).] When the NAD$^+$-thienodiazaborine complex is fitted into the active site of DHFR, there are some steric clashes between the sulfonyl group and the propyl tail of the diazaborine with parts of the enzyme surface. Nonetheless, there is sufficient space around the 2′OH of the nicotinamide ribose to envisage the formation of a linker between the ribose and a folate analog.

Analysis of the drug complex showed that the distance between the boron atom of the diazaborine and the 2′ hydroxyl of the nicotinamide ribose was ~1.7 Å, comparable with a B–O covalent bond length of 1.6 Å. The quality of the electron density map (particularly for the thienodiazaborine complex at 2.2 Å) implies that the errors in coordinates are very small, and thus we can be confident that the interaction between these two atoms is covalent. This conclusion is further supported by the unambiguous identification of the position of the hydroxyl oxygen to which the boron is linked, which can be seen to form part of a tetrahedral rather than a trigonal arrangement, as required if the boron forms four covalent bonds (Fig. 1, B and C). This finding provides a clear explanation for the strong inhibitory properties of the diazaborines and for the requirement of NAD$^+$ for diazaborine binding. The formation of the covalent bond further explains why the replacement of the B-N group in the diazaborine by an isoelectronic C-C unit in an isoquinoline analog showed no biological activity (*8*). The formation of the covalent bond in this case resembles the manner in which the boronic acid inhibitors of serine proteases act through the chemical modification of the active-site serine to give a covalently bound tetrahedral adduct (*9*).

The structure of the *E. coli* enzyme is closely related to that of its mycobacterial counterpart [Protein Data Bank (PDB) entry 1ENY (*1*); 40% sequence identity; 199 Cα atoms superimposed, root-mean-square

deviation (rmsd) 1.1 Å], particularly in the region of the active site, and also to that of *Brassica napus* ENR [PDB entry 1ENO (*10*); 33% sequence identity; 208 Cα atoms superimposed, rmsd 1.4 Å]. Examination of the structures of the *E. coli* and *M. tuberculosis* ENRs shows that their respective $Gly^{93} \rightarrow Ser$ (G93S) and $Ser^{94} \rightarrow Ala$ mutations, which lead to resistance to diazaborine (*11*) and isoniazid (*1*), respectively, map to regions close to the nucleotide-binding site. Modeling studies show that in the absence of changes to the main-chain torsion angles in the G93S mutant of *E. coli* ENR, the Cβ atom of the serine side chain would be unacceptably close to the two oxygens of the sulfonyl group of the diazaborine. Therefore, resistance to diazaborine is probably explained by the serine side chain of the G93S mutant encroaching into the drug-binding site and causing severe steric hindrance.

The position of the aromatic bicyclic ring of the diazaborine above the nicotinamide ring strongly resembles the model proposed for the binding of the enoyl substrate on the basis of studies on *B. napus* ENR (*10*), with the proposed position for the negatively charged oxygen of the enolate anion of the substrate close to that of the boron atom in the drug. Thus, the formation of a covalent bond between ENR and diazaborine generates a tight, noncovalently bound bisubstrate analog. No such good bisubstrate inhibitors have previously been described for NAD(P)-dependent oxidoreductases. Examples of this type designed to inhibit 3-hydroxy-3-methyl glutaryl (HMG) coenzyme A reductase were only very weak inhibitors of cholesterol biosynthesis, possibly because of the lack of a moiety to mimic the adenosine diphosphoribose, but more likely because of steric problems in the active site associated with the nature of the linkage that used the C-4 atom of the nicotinamide ring (*12*). In contrast, our study provides clear evidence for the type of linkage that may need to be created in order to synthesize a bisubstrate analog with the necessary geometry to occupy the active-site cleft. This may prove crucial in the design of a new generation of antibacterial agents against a range of drug-resistant organisms, including *M. tuberculosis*. However, given the inherent toxic potential of boron (*8*), the development of a range of inhibitors with minimal side effects will require the design of a preformed bisubstrate analog in which another atom is substituted for boron.

More widely, a number of NAD(P)-dependent oxidoreductases are known to be drug targets, including dihydrofolate reductase (DHFR), the target for the anticancer agent methotrexate (*13*); steroid 5α-reductase, the target for finasteride, used to treat benign prostatic hyperplasia (*14*); and inosine monophosphate dehydrogenase (IMPDH), the target for the immunosuppressant mycophenolic acid (MPA) (*15*). Structural analysis of members of the family of NAD(P)-dependent oxidoreductases has shown that the relative orientation of the nicotinamide ring, its associated ribose, and the enzyme active site are often closely related. Moreover, the catalytic oxidation-reduction cycle in these enzymes necessarily leads to a situation where the π electron system of a substrate approaches the face of the nicotinamide ring. Thus, for the subset of dehydrogenases where there is sufficient space in the structure around the 2′OH group of the nicotinamide ribose, there is an excellent opportunity to mimic the chemistry seen in the NAD^+-diazaborine complex in the synthesis of new enzyme inhibitors. For example, the superposition of the nucleotide-inhibitor complex of ENR into the active site of the nucleotide-substrate complex of DHFR indicates that linking a folate analog to the nicotinamide ribose is a distinct possibility, and such a strategy might be used in the design of new anticancer agents (Fig. 1D). Moreover, the similarity between the ENR-NAD^+-diazaborine complex and the orientation of the inosine-5′-monophosphate thioimidate intermediate and the inhibitor MPA in IMPDH (*15*) suggests that the 2′ hydroxyl of the inosine might be linked to the inhibitor in a similar manner; however, coordinates of the latter are not yet available for a more detailed comparison. These examples suggest that the use of the ribose hydroxyl to create a bisubstrate analog may find important applications in other areas of medicinal chemistry.

Table 1. X-ray data collection and phasing statistics. See (*6*) and (*7*) for descriptions of data sets.

Data set	Form A crystals				Form B crystals	
	Native-1	Native-2	Merged	Hg	Thieno	Benzo
Resolution (Å)	2.5	2.1	2.1	3.0	2.2	2.5
No. of observed reflections	114,615	86,550	113,658	20,674	76,176	45,376
No. of unique reflections	27,520	49,465	51,902	14,042	31,179	20,393
Completeness (%)	78	89	93	73	95	95
R_{merge}* (%)	7.1	3.8	5.8	7.7	5.8	5.7
Mean fractional isomorphous difference†				0.24		
No. of heavy atom sites				6		
Phasing power (acentric/centric)‡				1.4/1.0		
R_{Cullis} (acentric/centric)§				0.76/0.68		

*$R_{merge} = \Sigma_{hkl}|I_i - I_m|/\Sigma_{hkl}I_m$, where I_i and I_m are the observed intensity and mean intensity of related reflections, respectively. †Mean fractional isomorphous difference $= \Sigma\,||F_{PH}| - |F_P||/\Sigma\,|F_P|$, where F_{PH} and F_P are the structure factor amplitudes for derivative and native crystals, respectively. ‡Phasing power = $\langle F_H/\text{lack of closure}\rangle$. §$R_{Cullis}$ = ⟨lack of closure⟩/⟨isomorphous difference⟩.

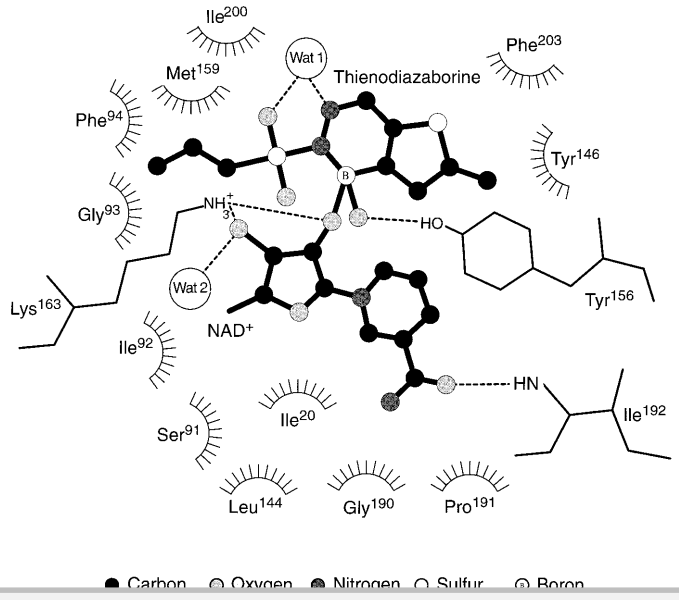

Fig. 2. Schematic representation of the interactions made by the NAD^+-thienodiazaborine complex with the enzyme surface and ordered solvent molecules. For NAD^+, only the nicotinamide ring and the nicotinamide ribose are shown. Hydrogen bonds are represented by dashed lines, hydrophobic contacts are shown as semicircular arcs, and Wat 1 and Wat 2 are two ordered solvent molecules. [Produced using LIGPLOT (*28*).]

REFERENCES AND NOTES

1. A. Banerjee *et al., Science* **263**, 227 (1994); A. Dessen, A. Quémard, J. S. Blanchard, W. R. Jacobs Jr., J. C. Sacchettini, *ibid.* **267**, 1638 (1995).
2. H. Bergler *et al., J. Biol. Chem.* **269**, 5493 (1994).
3. S. T. Cole, *Trends Microbiol.* **2**, 411 (1994).
4. G. Högenauer and M. Woisetschläger, *Nature* **293**, 662 (1981).
5. M. M. Kater, G. M. Koningstein, H. J. J. Nijkamp, A. R. Stuitje, *Plant Mol. Biol.* **25**, 771 (1994).
6. *Escherichia coli* ENR is a homotetramer ($M_r \sim 28{,}000$ per subunit) that was prepared from an overexpressing *E. coli* strain (*2, 5*). Crystals of the ENR-NAD$^+$ complex (crystal form A) belong to space group $P2_1$ and have unit cell dimensions of $a = 74.0$ Å, $b = 81.2$ Å, $c = 79.0$ Å, and $\beta = 92.9°$ with a tetramer in the asymmetric unit (*16*). Data were collected to 2.5 Å (Table 1, data set Native-1) on a twin San Diego Multiwire Systems (SDMS) area detector with a Rigaku RU-200 rotating anode source, and the data set was processed with SDMS software (*17*). Data were also collected to 2.1 Å (Table 1, data set Native-2) at the CLRC Daresbury Synchrotron and processed with the MOSFLM package (*18*), and the 2.1 and 2.5 Å data sets were then scaled and merged with CCP4 software (*19*). Initially, a model of *B. napus* ENR (*10*) was used as a basis for a molecular replacement solution of the structure, but the map, calculated after the model was refined with the program TNT (*20*), was not of sufficient quality to confidently assign residues in regions of structural differences between the *B. napus* and *E. coli* enzymes. Therefore, to solve the structure, we obtained a heavy-atom derivative by soaking an ENR-NAD$^+$ (form A) crystal for 1 hour in 0.1 mM ethylmercuriphosphate, 10 mM NAD$^+$, 20% (w/v) polyethylene glycol (molecular weight 400), and 100 mM acetate (pH 5.0). Derivative data were collected at the CLRC Daresbury Synchrotron to a resolution of 3 Å (Table 1, data set Hg) and were processed as above. The positions of the heavy atoms in this derivative were revealed by difference Fourier methods with the use of the approximate phases provided by the molecular replacement solution. The heavy-atom parameters were refined with the program MLPHARE (*21*) and resulted in a phase set with an overall mean figure of merit of 0.34 to 3 Å resolution. Using a map derived from these phases, we generated molecular masks for the molecule with the program MAMA (*22*) and performed 50 cycles of solvent flattening and fourfold molecular averaging with the program DM (*19, 23*). In the resultant electron density map, calculated from the averaged phases, we were able to find clear density for all but the first residue, the last four residues, and 10 residues from the loop joining β6 and α6; using the graphics program FRODO (*24*), we were able to build with confidence a model comprising 247 of the 262 amino acids of *E. coli* ENR. Several cycles of rebuilding and refinement gave a final *R* factor for the model of 0.157 (52,346 reflections in the range 10 to 2.1 Å, 7836 atoms including 324 water molecules), with an rmsd of 0.017 Å for bonds and 2.92° for angles [$R = \Sigma||F_{obs}| - |F_{calc}||/\Sigma|F_{obs}|$), where $|F_{obs}|$ and $|F_{calc}|$ are the observed and calculated structure factor amplitudes, respectively]. The average *B* factor for the tetramer is 30 Å^2 (24 Å^2 for main-chain atoms), where $B = 8\pi^2(\bar{\mu}^2)$ and $\bar{\mu}$ is the mean square displacement of the atomic vibration.
7. Crystals of the ENR-NAD$^+$-diazaborine complex (crystal form B) belong to space group $P6_122$ and have unit cell dimensions of $a = b = 80.9$ Å, $c = 328.3$ Å, $\alpha = \beta = 90°$, and $\gamma = 120°$ for the thienodiazaborine complex, and $a = b = 80.6$ Å, $c = 325.3$ Å, $\alpha = \beta = 90°$, and $\gamma = 120°$ for the benzodiazaborine complex with a dimer in the asymmetric unit (*16*). Data sets were collected on the ENR-NAD$^+$-thienodiazaborine complex to 2.2 Å and on the ENR-NAD$^+$-benzodiazaborine complex to 2.5 Å (Table 1, data sets Thieno and Benzo) at the CLRC Daresbury Synchrotron and were processed as above. The structures of both ENR-NAD$^+$-diazaborine complexes were solved independently by molecular replacement with the use of an appropriate dimer from the *E. coli* ENR-NAD$^+$ structure and were refined against their respective data sets with the program TNT (*20*). The initial electron density maps were readily interpretable and unambiguous density could be observed for the location of the diazaborine compounds, which were then incorporated into the refinement. Clear density could be found for all but the first residue and the last four residues. Refinement of the thienodiazaborine complex gave a final *R* factor of 0.191 (30,825 reflections in the range 10 to 2.2 Å, 3936 atoms), with an rmsd of 0.012 Å for bonds and 2.9° for angles. The average *B* factor for the dimer is 27 Å^2 (22 Å^2 for main-chain atoms, 20 Å^2 for diazaborine atoms). Refinement of the benzodiazaborine complex gave a final *R* factor of 0.169 (20,204 reflections in the range 10 to 2.5 Å, 3930 atoms), with an rmsd of 0.013 Å for bonds and 2.7° for angles. The average *B* factor for the dimer is 24 Å^2 (20 Å^2 for main-chain atoms, 20 Å^2 for diazaborine atoms). For the ENR-NAD$^+$ complex and the ENR-NAD$^+$-thienodiazaborine complex, 244 Cα atoms superimpose with an rmsd of 0.3 Å, whereas for the two ENR-NAD$^+$-diazaborine complexes, 256 Cα atoms superimpose with an rmsd of 0.2 Å.
8. M. A. Grassberger, F. Turnowsky, J. Hildebrandt, *J. Med. Chem.* **27**, 947 (1984).
9. S. Zhong, F. Jordan, C. Kettner, L. Polgar, *J. Am. Chem. Soc.* **113**, 9429 (1991).
10. J. B. Rafferty *et al., Structure* **3**, 927 (1995).
11. H. Bergler, G. Högenauer, F. Turnowsky, *J. Gen. Microbiol.* **138**, 2093 (1992).
12. C. Taillefumier, D. de Fornel, Y. Chapleur, *Bioorg. Med. Chem. Lett.* **6**, 615 (1996).
13. J. T. Bolin, D. J. Filman, D. A. Matthews, R. C. Hamlin, J. Kraut, *J. Biol. Chem.* **257**, 13650 (1982); C. Bystroff, S. J. Oatley, J. Kraut, *Biochemistry* **29**, 3263 (1990).
14. H. G. Bull *et al., J. Am. Chem. Soc.* **118**, 2359 (1996).
15. M. D. Sintchak *et al., Cell* **85**, 921 (1996).
16. C. Baldock *et al., Acta Crystallogr.,* in press.
17. R. Hamlin, *Methods Enzymol.* **114**, 416 (1985); A. J. Howard, C. Nielson, N. H. Xuong, *ibid.,* p. 452; N. H. Xuong, C. Nielson, R. Hamlin, D. Anderson, *J. Appl. Crystallogr.* **18**, 342 (1985).
18. A. G. W. Leslie, *Joint CCP4 and ESF-EACBM Newsletter on Protein Crystallography No. 26* (SERC Daresbury Laboratory, Warrington, UK, 1992).
19. Collaborative Computational Project No. 4, *Acta Crystallogr.* **D50**, 760 (1994).
20. D. E. Tronrud, L. F. Ten Eyck, B. W. Matthews, *ibid.* **A43**, 489 (1987).
21. Z. Otwinowski, in *Proceedings of the CCP4 Study Weekend,* W. Wolf, P. R. Evans, A. G. W. Leslie, Eds. (SERC Daresbury Laboratory, Warrington, UK, 1991), p. 80.
22. G. J. Kleywegt and T. A. Jones, *ESF/CCP4 Newsletter No. 28* (1993), p. 56.
23. K. Cowtan, *ESF/CCP4 Newsletter No. 31* (1994), p. 34.
24. T. A. Jones, *J. Appl. Crystallogr.* **11**, 268 (1978).
25. T. E. Ferrin, C. C. Huang, L. E. Jarvis, R. Langridge, *J. Mol. Graphics* **6**, 13 (1988).
26. R. Esnouf, personal communication.
27. P. J. Kraulis, *J. Appl. Crystallogr.* **24**, 946 (1991).
28. A. C. Wallace, R. A. Laskowski, J. M. Thornton, *Protein Eng.* **8**, 127 (1995).

29. We thank the support staff at the Synchrotron Radiation Source at Daresbury Laboratory for assistance with station alignment. Supported by grants from the UK Biotechnology and Biological Sciences Research Council (BBSRC) and Medical Research Council (D.W.R. and A.R.S.). C.B. is funded by a Zeneca Agrochemicals–supported CASE award. J.B.R. is a BBSRC David Phillips Research Fellow. The Krebs Institute is a designated BBSRC Biomolecular Science Centre.

2 August 1996; accepted 15 October 1996

Orientation Maps of Subjective Contours in Visual Cortex

Bhavin R. Sheth, Jitendra Sharma, S. Chenchal Rao, Mriganka Sur*

Responses to subjective contours in visual cortical areas V1 and V2 in adult cats were investigated by optical imaging of intrinsic signals and single-unit recording. Both V1 and V2 contain maps of the orientation of subjective gratings that have their basis in specific kinds of neuronal responses to subjective orientations. A greater proportion of neurons in V2 than in V1 show a robust response to subjective edges. Through the use of subjective stimuli in which the orientation of the luminance component is invariant, an unmasked V1 response to subjective edges alone can be demonstrated. The data indicate that the processing of subjective contours begins as early as V1 and continues progressively in higher cortical areas.

Contours that are perceived under stimulus configurations in which the stimulus lacks any physical discontinuity (such as a luminance border) are termed subjective or illusory contours. Subjective contours and subjective shapes can be perceived in a manner analogous to the perception of luminance contours and shapes (*1*), suggesting that subjective and luminance contours might be processed in similar manner, perhaps by similar neural substrates. A subset of neurons in V2 of monkeys has been shown to respond to subjective edges (*2*). In addition, cells in monkey V1 have been reported to respond to subjective edges (*3*); however, the stimuli used were different from classical subjective stimuli because they had a luminance gradient across the putative "subjective" edge. Thus, the question of whether or not V1 neurons respond to subjective stimuli remains unresolved. Further-

Department of Brain and Cognitive Sciences, Massachusetts Institute of Technology (MIT), Cambridge, MA 02139, USA.

*To whom correspondence should be addressed at Department of Brain and Cognitive Sciences, MIT, E25-235 Cambridge, MA 02139, USA. E-mail: msur@wccf.mit.edu